Semarak International Journal of Nanotechnology

Journal homepage:
https://semarakilmu.com.my/journals/index.php/sijn/index
ISSN: XXX-XXX

Nanostructuring of Additively Manufactured 316L Stainless Steel via High Pressure Torsion: Microstructural and Hardness Inhomogeneities at Low Torsional Strain Levels

Shahir Mohd Yusuf[1,*], Nur Hidayah Musa[1], Nong Gao[2]

[1] Engineering Materials and Structures iKohza, Malaysia-Japan International Institute of Technology (MJIIT), UTM Kuala Lumpur, 54100 Kuala Lumpur, Malaysia
[2] Faculty of Engineering and Physical Sciences, University of Southampton, Southampton SO17 1 BJ, United Kingdom

ARTICLE INFO

Article history:
Received 3 April 2024
Received in revised form 15 April 2024
Accepted 28 May 2024
Available online 10 June 2024

Keywords:
nanostructures; high pressure torsion; additive manufacturing; 316L stainless steel; ultrafine grained microstructures; nano-grained microstructures; hardness

ABSTRACT

High-pressure torsion (HPT) is a severe plastic deformation (SPD) process that produces ultrafine-grained (UFG) and/or nano-grained (NG) microstructures in bulk disk-shaped metallic materials to enhance their mechanical properties, accompanied by inhomogeneous microstructures and hardness distributions across the disk radius. Although such inhomogeneity due to the radial dependency of HPT process is well-documented in conventionally wrought and cast HPT-processed metals and alloys, it has not been studied in their additively manufactured counterparts. Thus, this study aims to investigate the inhomogeneous distribution of microstructures and hardness values across HPT-processed disk-shaped 316L stainless steel (316L SS) samples additively manufactured by laser powder bed fusion (L-PBF). The disk samples are subjected to 1/4 and 1 HPT revolution, followed by extensive microstructural characterisation and Vickers hardness (HV) measurements. The results show: (i) fine micron (18±17 µm) and UFG (118±25 nm) microstructures at the central ($0<r<2.5$ mm) and peripheral ($r>3$ m) disk regions, respectively after 1/4 HPT revolution, and (ii) UFG (980±500 nm) and true NG (68±15 nm) microstructures at the central and peripheral disk regions, respectively after 1/4 HPT revolution. Unsurprisingly, a 2- to 3-fold hardness increase (430 – 550 HV) is observed after HPT processing compared to the as-received L-PBF AM 316L SS (200 – 250 HV) with the central disk area consistently exhibits relatively lower hardness values compared to the disk peripheries. The results present an exciting potential avenue to tailor or enhance the properties of additively manufactured metals and alloys such as strength-ductility synergy by introducing gradient nanostructures through the microstructural inhomogeneity attained via HPT.

1. Introduction

316L stainless steel (316L SS) is a common austenitic SS alloy commonly used in the biomedical, marine, food and beverage, and nuclear industries due to its excellent corrosion resistance, low neutron absorption, and good ductility. However, the relatively modest ultimate tensile strength of

* *Corresponding author.*
E-mail address: shahiryasin@utm.my

316L SS, <600 MPa resulting from its relatively coarse austenitic grains (>60 µm) restricts its applications for advanced structural applications such as those subjected to high loadings and harsh environments as discussed in previous studies [1–3]. In fact, its low carbon content (typically <0.03 wt.%) mean that this alloy could not be heat treated to improve its strength, unlike Al and Ni alloys that can be strengthened by various heat treatment procedures through the precipitation hardening mechanism as has been shown in numerous studies [4–6]. Thus, the only viable approach for increasing the strength of 316L SS is via grain refinement route based on the Hall-Petch relationship (reducing grain size to improve yield/tensile strength), e.g. through cold working. Nevertheless, cold working processes such as rolling, forging, and other conventional forming processes could only yield limited grain refinement (within the range of tens of microns) due to their limited capabilities of inducing plastic deformation as demonstrated by Xu *et al.,* [7]. Thus, further grain refinements down to the ultrafine grained (UFG) regions (grain sizes ranging from 100 nm – 1 µm) and/or true nano-grained (NG) regime (<100 nm), perhaps via higher degrees of plastic deformation is deemed necessary to achieve the intended goal for this alloy to be used in advanced structural applications.

Fortunately, such an approach exists through high-pressure torsion (HPT), a well-known severe plastic deformation (SPD) technique. It involves the application of extreme torsional strain levels on disk-shaped metallic materials that can produce UFG and/or NG microstructures by introducing dense dislocation networks and other nano-scale microstructural features as has been shown in previous studies [8–10]. In HPT process, thin disk samples are placed within two large anvils whereby the lower anvil is initially pushed up to provide large hydrostatic pressures (typically up to 6 GPa) before being rotated to impose torsional shear strains onto the disks. The equivalent von Mises strain, $\varepsilon_{eq.}$ Imposed by HPT is typically estimated by the following equation described by Vorhauer *et al.* [11]: $\varepsilon_{eq.} = 2\pi Nr/h$, where *N* is the number of HPT revolutions, *r* is the radius of the disk, and *h* is the disk thickness. Based on this equation, in theory there should exist variations in applied strain values across the radius of the disk, i.e. zero strain at the centre of the disk in which *r*=0 and increasing strain towards the edge of the disk. This observation therefore implies a radial dependency in the HPT process, possibly suggesting inhomogeneity in the microstructures attained and the resulting hardness values that may vary considerably as a function of radial location of the disk based on the strain gradient plasticity theory proposed by Ashby [12]. Indeed, previous studies reviewed by Kawaski *et al*., [13] that (i) not only the strain at *r*=0 is not zero such that small deformation occurs at least, evidenced by the hardness increase compared to the non-HPTed samples, but also (ii) different levels of grain refinements and hardness values across the disk radius; i.e. UFG microstructures and relatively lower hardness at central disk areas (0<*r*<2.5 mm) and NG microstructures at significantly higher hardness closer to the peripheral regions (*r*>3 mm), particularly at lower strains during the early deformation stages, e.g. *N*=1/4 to 1.

Recently, efforts to enhance the mechanical (hardness, yield and tensile strength and functional (e.g. corrosion, wear, etc.) in additively manufactured metallic materials by applying HPT process have been initiated by Mohd Yusuf *et al*., [14–19] for 316L SS and Al Zubaydi *et al*., [20,21] for AlCuMg. However, these studies only reported on overall enhancements in the mechanical and functional properties by discussing the general UFG and/or NG microstructures formed after HPT, rather than focusing on the inhomogeneous microstructures formed at the central and peripheral disk regions that contribute to such improvements in the properties. Thus, in this study, HPT processing is initially applied to 316L SS samples additively manufactured by laser powder bed fusion (L-PBF) from *N*=1/4 to 1, i.e. lower strain levels. This is followed by detailed microstructural characterisation of the UFG and NG microstructures formed as well as hardness analysis at the central and peripheral areas of the disk to address the inhomogeneity aspect of HPT processing on L-PBF 316L SS at the early deformation stages.

2. Methodology

At first, L-PBF process is used to additively manufacture a 316L SS cylindrical rod (200 mm length, 10 mm diameter) by using a Concept Laser M2 LaserCusing machine with the following processing parameters; laser power, *P*: 200 W, scan speed, *v*: 1600 mm s^{-1}, layer thickness, *d*: 30 µm, scan line spacing, *h*: 150 µm, and scan strategy: 5×5 mm islands. In preparation for HPT processing, the rod is precisely sliced into thin disks of 1 mm through wire electrical discharge machining (EDM) and further ground to ~ 0.85 mm by using 800 grits of SiC paper. The disks are then subjected to 1/4 and 1 HPT revolutions (*N*=1/4 and *N*=1, respectively) in a quasi-constrained condition under 6 GPa of pressure and speed of 1 rpm. The schematic of HPT process is adapted from Zhang *et al.,* [22] and shown in Figure 1.

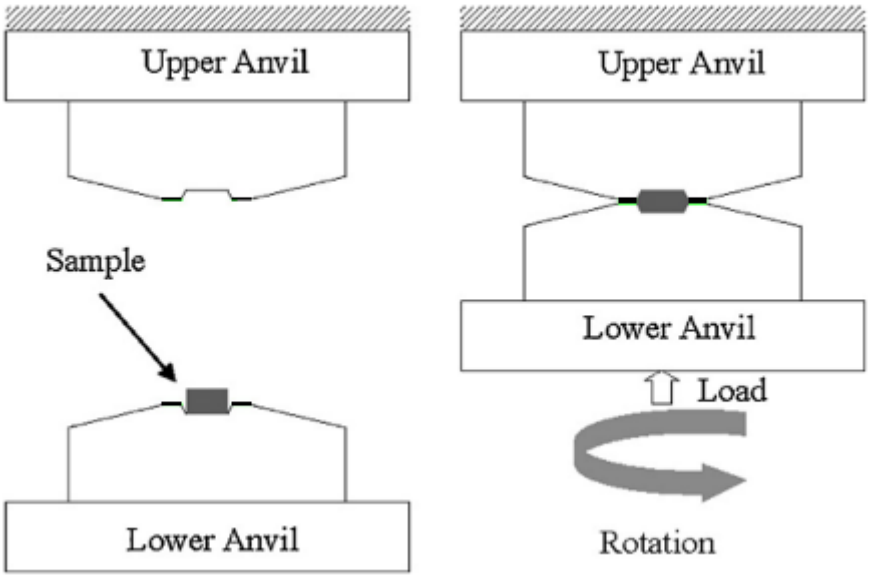

Fig. 1. Schematic of HPT process taken from Zhang *et al*., [22]

After HPT processing, the disks are subjected to typical sample preparation procedures for scanning electron microscopy (SEM) observations, including grinding (800 – 4000 grits SiC paper), polishing (1 µm diamond suspension), and etching (Kalling's No. 2 reagent). SEM observations are conducted at the central (0<*r*<2.5 mm) and peripheral (*r*>3 mm) disk areas. It is known that for nanostructured metallic materials, advanced characterisation techniques are required to ascertain the UFG and UG microstructures, Thus, electron backscattered diffraction (EBSD) analysis is conducted at the central disk areas and transmission electron microscopy (TEM) observations is carried out at the periphery as per the custom of numerous HPT-related studies [23–25]. For EBSD, the disks are electropolished in 80:20 ratio methanol-perchloric acid mixture solution for 18 s at 16 V and 0.5 A. Subsequently, EBSD images are taken at areas of 100×100 µm (step size 0.1 µm) that covers >100 grains each. For TEM, the disks are further mechanically ground to 80 µm thickness before 3 mm smaller disks are extracted to be dimpled using a dimple grinder and then polished into thin foils by using a precision ion poilishing system (PIPS). The intercept method described by Thorvaldsen [26] is used to measure the average grain sizes based on 300 grains in 20 TEM images each. Finally, the hardness values are analysed based on the results of Vickers microhardness (HV) measurements taken in a rectilinear grid pattern throughout the disk surface in a previous study by Mohd Yusuf *et al.,* [18] and correlated with the microstructures observed in this study.

3. Results and Discussions

3.1 Microstructural Characterisation

Figure 2 displays the representative microstructures of the as-received and HPT-processed L-PBF AM 316L SS. In particular, the EBSD map in Figure 2(a) exhibits a mix of coarse and fine grains averaging 40 ± 30 µm formed after L-PBF (as-received condition) in almost square-like patterns corresponding to the 'island' scan strategy used during the AM fabrication process. The inverse pole (IPF) figure (inset of Figure 2(a) suggests generally random grain growth without any preferred orientation and therefore no dominant texture as explained in various studies [27–32].

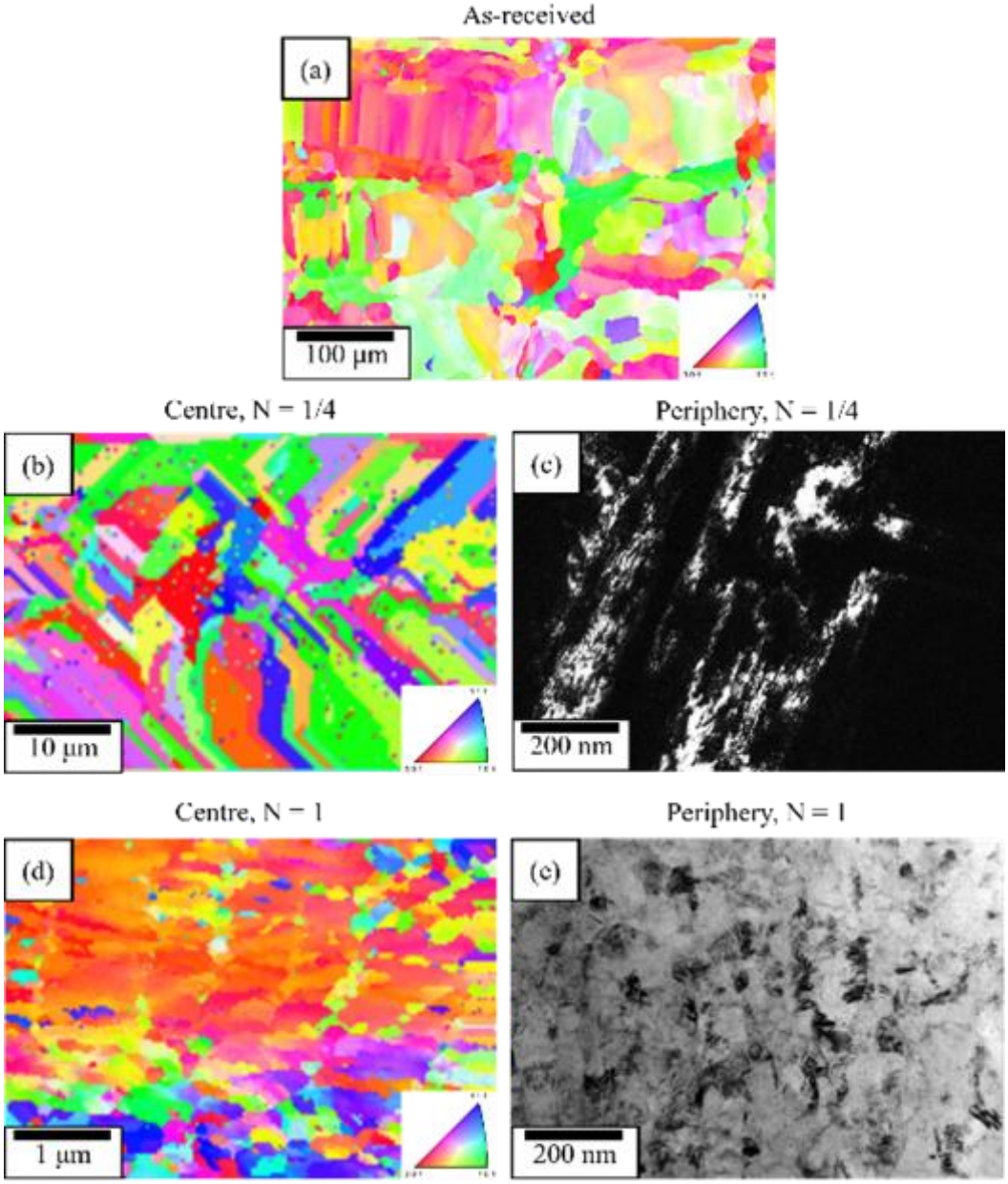

Fig. 2. (a) Coarse-grained microstructures in the as-received samples, and UFG//NG microstructures at the central and peripheral disk regions after (b-c) *N*=1/4 and (d-e) *N*=1

However, the central and peripheral regions begin to exhibit changes in microstructures after 1/4 and 1 HPT evolutions. The impact of the torsional strain imposed by HPT is clearly pronounced at the disk centre after *N* = 1/4 ($0<\varepsilon_{eq.}<4.6$) by the visibly elongated grains (Fig. 2(b)). Here, the average grain size is 18±17 µm, indicating that the grains are still within the fine micron range and has not entered the UFG domain yet. Contrastingly, the TEM image of the representative peripheral disk area in Fig. 2(c) ($5.5<\varepsilon_{eq.}<9.2$) exhibit similarly elongated, but sub-micron sized grains suggest that UFG microstructures could already be formed even at the early HPT deformation stage, i.e. after 1/4 revolution in this case. Indeed, measurements through the intercept method reveal that the average grain size obtained after *N*=1/4 at the peripheral disk region is 118±25 nm. As the number of HPT revolutions increase to *N*=1, the fraction of elongated grains reduces at the disk centre ($0< \varepsilon_{eq.}<18.5$), and equiaxed sub-micron grains (UFG microstructure) start to form with an average intercept grain size of 980±500 nm (Fig. 2(d)). On the other hand, nano-scale grains are formed at the peripheral area after1 HPT revolution ($22.2<\varepsilon_{eq.}<37$) as shown in Fig. 2(e). However, the grain boundaries appear ill-defined and somewhat wavy and diffused at this stage, a microstructural phenomenon commonly observed in HPT-, SPD-processed metallic materials in general that is indicative of high-energy non-equilibrium boundaries and an excess of extrinsic dislocations as explained by Ma *et al.,* [33]. The average grain size here is determined as 68±15 nm, exhibiting true NG microstructures attained at the peripheral region after 1 HPT revolution. Nevertheless, Mohd Yusuf *et al*., [34]. explained that the grain refinements in HPT-processed L-PBF AM 316L SS at early deformation stages can be attributed to the competing mechanisms of dislocation generation/multiplication, primary and secondary nanotwin formations and shear banding of the nanotwins.

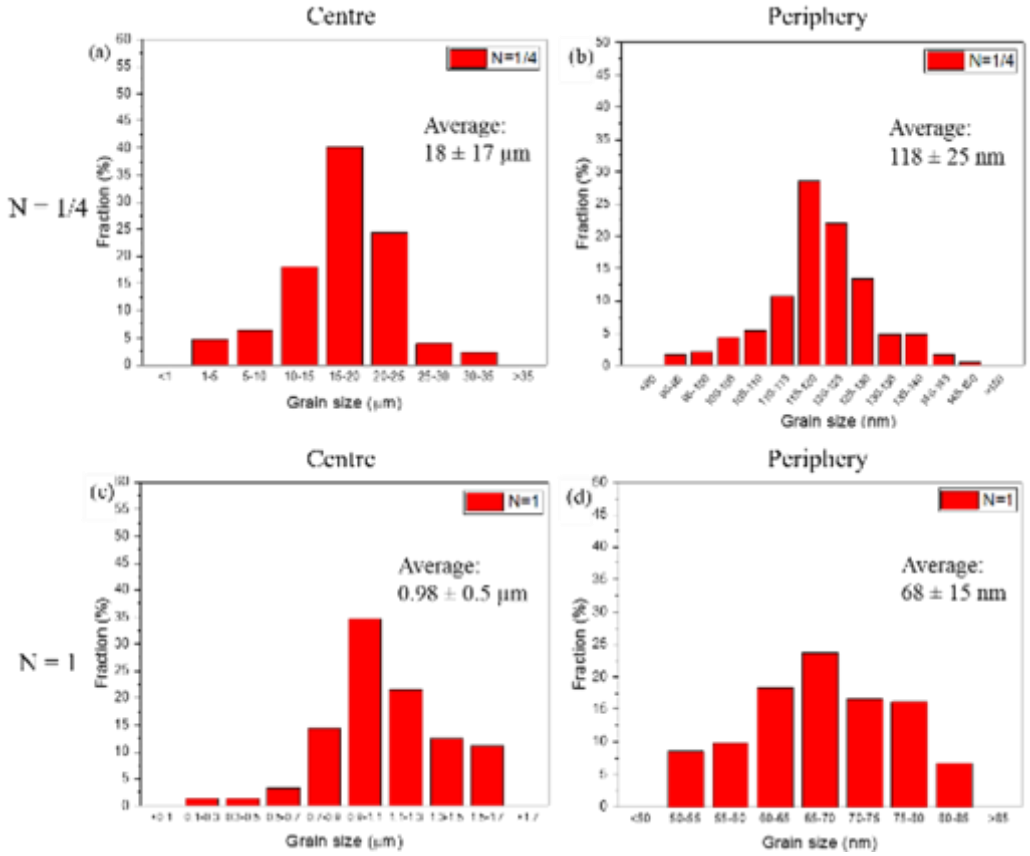

Fig. 3. Inhomogeneity in grain size distributions at disk centre (0<*r* <2.5 mm) and periphery (*r*> 3 mm) after 1/4 and 1 HPT revolutions.

Meanwhile, Figure 3 exhibits the distribution of grain sizes at the central and peripheral disk region after 1/4 and 1 HPT revolutions. The grain sizes remain in the fine micron region (1–35 µm) at the central area despite the refinement after 1/4 HPT revolution (0 <$\varepsilon_{eq.}$<4.6) as shown in Figure 3(a), but UFG and NG microstructures ranging from 90 – 150 nm are already formed at the periphery at this early deformation stage (5.5<$\varepsilon_{eq.}$<9.2). Increased torsional strain to 1 HPT revolution result in further grain refinements at the central disk region (0<$\varepsilon_{eq.}$<18.5) down to 0.1 – 2 µm, while true nanostructured regime (53 – 83 nm) is reached at the periphery (22.2<$\varepsilon_{eq.}$<37) as respectively displayed in Figure 3(c) and (d). Thus, the microstructural observations and analysis provided in Figure 2 and 3 clearly show inhomogeneous microstructural formation and distribution in the HPT-processed material at early deformation stages, correlating well with the studies reviewed by Kawasaki *et al.,* [13] previously. Consequently, these would also suggest certain levels of inhomogeneity in the resulting hardness values at the central and peripheral disk regions.

3.2 Vickers Microhardness Distribution

Figure 4 shows colour-coded contour maps of HV measurements taken in a rectilinear grid pattern on the as-received and HPT-processed L-PBF AM 316L SS conducted previously by Mohd Yusuf *et al.,* [18]. The X- and Y- positions are arbitrarily assigned, but the coordinate (0,0) represents the dead centre of the disk (*r*=0). Meanwhile, the colour key at the right side of Figure 4 indicates the range of HV values.

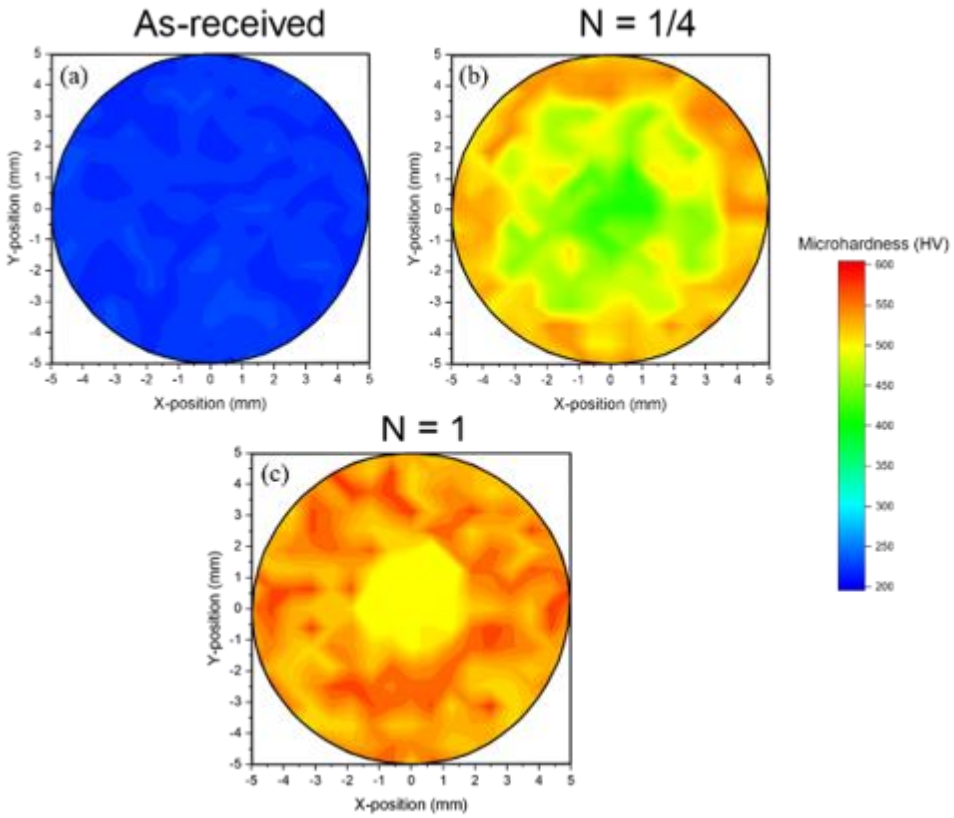

Fig. 4. HV distribution throughout the surface of as-received and HPT-processed L-PBF AM 316L SS presented as colour-coded contour maps based on result of Mohd Yusuf *et al.,* [18].

A homogeneous distribution of HV values can be observed for the as-received disk, ranging from 200 – 250 HV. The average hardness, 220 HV is higher than conventional wrought/cast 316L SS, but is common for 316L SS fabricated by L-PBF AM. This phenomenon has been attributed to the novel microstructures formed resulting from the high cooling rates (10^5 – 10^7 Ks^{-1}) compared to <10^3 Ks^{-1} in conventional approaches and also the layer-wise scan strategy involved during the fabrication process as explain in previous studies [35–37]. Nevertheless, inhomogeneous hardness distributions throughout the surface of the disks can be observed after 1/4 and 1 HPT revolutions as expected, consistent with the radial dependency of HPT process described previously. After N=1/4, the HV values at the central area ranges between 430 – 480 HV, whereas the peripheral region exhibits hardness between 500 – 540 HV (Fig. 4(b)). With increasing number of HPT revolution to N=1, the hardness values continue to increase to ~500 HV centrally, whereas the periphery only experiences marginal increment to ~ 550 HV (Fig. 4(c)). Nevertheless, the rapid ~2 to 3-fold increase in hardness values at the early HPT deformation stages (N=1/4 to 1) in this study can be ascribed to the significant work hardening that results in grain refinement, dislocation generation/multiplication and as reported in various literature [38–40]. These results highlight the effectiveness of HPT processing in producing UFG/NG microstructures that significantly enhances the hardness, and possibly yield and tensile strengths compared to conventional plastic deformation approaches such as rolling and forging. Another interesting implication from the outcomes of this study is the exciting possibility of introducing gradient nanostructures in additively manufactured metallic materials through the microstructural inhomogeneity resulting from HPT or other SPD processes such as equal channel angular pressing (ECAP) and accumulative roll bonding (ARB). Numerous studies have shown the advantages of gradient-nanostructured materials, including excellent strength-ductility synergy, coupled with improved functional properties, e.g. corrosion and wear as evident in various literature [41–44]. Therefore, this presents and interesting opportunity to embark on studying the effects of gradient nanostructures resulting from the microstructural homogeneity via HPT processing on the strength and ductility, as well as the resulting functional properties of L-PBF AM materials in the future.

4. Conclusions

In the present study, the microstructural and hardness inhomogeneities in L-PBF AM-fabricated 316L SS processed by HPT through 1/4 and 1 revolution are investigated by extensive microstructural characterisation, and the UFG/NG microstructures are correlated with Vickers microhardness (HV) measurements from a previous study. The following conclusions can be drawn based on the results of this study:

i. Microstructural inhomogeneity is observed after HPT processing, in which the central disk areas (0<r<2.5 mm) reveal smaller grain sizes compared to those at the peripheral regions (r>3 mm).
ii. After 1/4 HPT revolution, the average grain size at the central disk area is still in the fine micron region (18±17 μm), whereas the peripheries exhibit UFG grain microstructures (average grain size: 118±25 nm).
iii. After 1 HPT revolution, UFG microstructures with an average grain size of 980±500 nm is attained at the disk centre, whereas true NG microstructures (average grain size: 68±15 nm) are observed at the peripheral region.
iv. The microstructural inhomogeneity after HPT processing is accompanied by an inhomogeneous increase in HV values at the central and peripheral disk regions.

v. The microstructural and hardness inhomogeneities can be attributed to the radial dependency of HPT processing that results in competing mechanisms of grain refinement, dislocation generation/multiplication, and primary/secondary nanotwin formation.

Acknowledgement
This work was funded by the Ministry of Higher Education (MOHE) Malaysia under the Fundamental Research Grant Scheme (FRGS /1/2021/TK0/UTM/02/84).

References

[1] Fitriyana, Deni Fajar, Samsudin Anis, Abdul Rachman Al Qudus, Mirza Aufa Nugraha Lakuy, Rifky Ismail, Sri Nugroho, Gunawan Dwi Haryadi, Athanasius Priharyoto Bayuseno, and Januar Parlaungan Siregar. "The Effect of Post-Heat Treatment on The Mechanical Properties of FeCrBMnSi Coatings Prepared by Twin Wire Arc Spraying (TWAS) Method on Pump Impeller From 304 Stainless Steel." *Journal of Advanced Research in Fluid Mechanics and Thermal Sciences* 93, no. 2 (2022): 138-147. https://doi.org/10.37934/arfmts.93.2.138147

[2] Abbud, Luay Hashem, Zaid S. Kareem, and Hyder H. Balla. "Thermal Effect of Welding Processes on A Steel Plate Subjected to Dynamic Load." *Journal of Advanced Research in Fluid Mechanics and Thermal Sciences* 67, no. 2 (2020): 13-26.

[3] Hidayah Musa, Nur, Nurainaa Mazlan, Shahir Mohd Yusuf, Nur Azmah Nordin, Saiful Amri Mazlan, and Nong Gao. "High densification level and hardness values of additively manufactured 316L stainless steel fabricated by fused filament fabrication." *Journal of Advanced Research in Applied Sciences and Engineering Technology* 34, no. 2 (2023): 144-152. https://doi.org/10.37934/araset.34.2.144152

[4] Shakil, S. I., A. Hadadzadeh, B. Shalchi Amirkhiz, H. Pirgazi, M. Mohammadi, and M. Haghshenas. "Additive manufactured versus cast AlSi10Mg alloy: Microstructure and micromechanics." *Results in Materials* 10 (2021): 100178. https://doi.org/10.1016/j.rinma.2021.100178

[5] Li, Wei, Shuai Li, Jie Liu, Ang Zhang, Yan Zhou, Qingsong Wei, Chunze Yan, and Yusheng Shi. "Effect of heat treatment on AlSi10Mg alloy fabricated by selective laser melting: Microstructure evolution, mechanical properties and fracture mechanism." *Materials Science and Engineering: A* 663 (2016): 116-125. https://doi.org/10.1016/j.msea.2016.03.088

[6] Chlebus, E., K. Gruber, B. Kuźnicka, J. Kurzac, and T. Kurzynowski. "Effect of heat treatment on the microstructure and mechanical properties of Inconel 718 processed by selective laser melting." *Materials Science and Engineering: A* 639 (2015): 647-655. https://doi.org/10.1016/j.msea.2015.05.035

[7] Xu, Deming, Xiangliang Wan, Jianxin Yu, Guang Xu, and Guangqiang Li. "Effect of cold deformation on microstructures and mechanical properties of austenitic stainless steel." *Metals* 8, no. 7 (2018): 522. https://doi.org/10.3390/met8070522

[8] Mavlyutov, Aydar, Alexey Evstifeev, Darya Volosevich, Marina Gushchina, Artem Voropaev, Oleg Zotov, and Olga Klimova-Korsmik. "The Effect of Severe Plastic Deformation on the Microstructure and Mechanical Properties of Composite from 5056 and 1580 Aluminum Alloys Produced with Wire Arc Additive Manufacturing." *Metals* 13, no. 7 (2023): 1281. https://doi.org/10.3390/met13071281

[9] Li, Zhuoliang, Hua Ding, Yi Huang, and Terence G. Langdon. "An Evaluation of the Mechanical Properties, Microstructures, and Strengthening Mechanisms of Pure Mg Processed by High-Pressure Torsion at Different Temperatures." *Advanced Engineering Materials* 24, no. 10 (2022): 2200799. https://doi.org/10.1002/adem.202200799

[10] Wang, Zhi-Rui, Ping-Zhan Si, Jihoon Park, Chul-Jin Choi, and Hong-Liang Ge. "A review of ultrafine-grained magnetic materials prepared by using high-pressure torsion method." *Materials* 15, no. 6 (2022): 2129. https://doi.org/10.3390/ma15062129

[11] Vorhauer, Andreas, and Reinhard Pippan. "On the homogeneity of deformation by high pressure torsion." *Scripta Materialia* 51, no. 9 (2004): 921-925. https://doi.org/10.1016/j.scriptamat.2004.04.025

[12] Ashby, M. F. "The deformation of plastically non-homogeneous materials." *The Philosophical Magazine: A Journal of Theoretical Experimental and Applied Physics* 21, no. 170 (1970): 399-424. https://doi.org/10.1080/14786437008238426

[13] Kawasaki, Megumi, Roberto B. Figueiredo, and Terence G. Langdon. "Twenty-five years of severe plastic deformation: recent developments in evaluating the degree of homogeneity through the thickness of disks processed by high-pressure torsion." *Journal of Materials Science* 47 (2012): 7719-7725. https://doi.org/10.1007/s10853-012-6507-y

[14] Yusuf, Shahir Mohd, Mengyan Nie, Ying Chen, Shoufeng Yang, and Nong Gao. "Microstructure and corrosion

performance of 316L stainless steel fabricated by Selective Laser Melting and processed through high-pressure torsion." *Journal of Alloys and Compounds* 763 (2018): 360-375. https://doi.org/10.1016/j.jallcom.2018.05.284

[15] Yusuf, Shahir Mohd, Ying Chen, Shoufeng Yang, and Nong Gao. "Microstructural evolution and strengthening of selective laser melted 316L stainless steel processed by high-pressure torsion." *Materials Characterization* 159 (2020): 110012. https://doi.org/10.1016/j.matchar.2019.110012

[16] Mohd Yusuf, Shahir, Ying Chen, and Nong Gao. "Influence of high-pressure torsion on the microstructure and microhardness of additively manufactured 316L stainless steel." *Metals* 11, no. 10 (2021): 1553. https://doi.org/10.3390/met11101553

[17] Yusuf, Shahir Mohd, Daryl Lim, Ying Chen, Shoufeng Yang, and Nong Gao. "Tribological behaviour of 316L stainless steel additively manufactured by laser powder bed fusion and processed via high-pressure torsion." *Journal of Materials Processing Technology* 290 (2021): 116985. https://doi.org/10.1016/j.jmatprotec.2020.116985

[18] Mohd Yusuf, Shahir, Ying Chen, Shoufeng Yang, and Nong Gao. "Micromechanical Response of Additively Manufactured 316L Stainless Steel Processed by High-Pressure Torsion." *Advanced Engineering Materials* 22, no. 10 (2020): 2000052. https://doi.org/10.1002/adem.202000052

[19] Mohd Yusuf, Shahir, Ying Chen, Nur Hidayah Musa, Nurainaa Mazlan, Nur Azmah Nordin, Nurhazimah Nazmi, Saiful Amri Mazlan, and Nong Gao. "Elimination of porosity in additively manufactured 316L stainless steel by high-pressure torsion." *The International Journal of Advanced Manufacturing Technology* 123, no. 3 (2022): 1175-1187. https://doi.org/10.1007/s00170-022-10228-w

[20] Al-Zubaydi, Ahmed SJ, Nong Gao, Shuncai Wang, and Philippa AS Reed. "Microstructural and hardness evolution of additively manufactured Al–Si–Cu alloy processed by high-pressure torsion." *Journal of Materials Science* 57, no. 19 (2022): 8956-8977. https://doi.org/10.1007/s10853-022-07234-4

[21] Al-Zubaydi, Ahmed SJ, Nong Gao, Jan Dzugan, Pavel Podany, Sandeep Sahu, Deepak Kumar, Ying Chen, and Philippa AS Reed. "The hot deformation behaviour of laser powder bed fusion deposited Al–Si–Cu alloy processed by high-pressure torsion." *Journal of Materials Science* 57, no. 43 (2022): 20402-20418. https://doi.org/10.1007/s10853-022-07847-9

[22] Zhang, Jiuwen, Nong Gao, and Marco J. Starink. "Al–Mg–Cu based alloys and pure Al processed by high pressure torsion: The influence of alloying additions on strengthening." *Materials Science and Engineering: A* 527, no. 15 (2010): 3472-3479. https://doi.org/10.1016/j.msea.2010.02.016

[23] Tirsatine, Kamel, Hiba Azzeddine, Yi Huang, Thierry Baudin, Anne-Laure Helbert, François Brisset, Djamel Bradai, and Terence G. Langdon. "An EBSD analysis of Fe-36% Ni alloy processed by HPT at ambient and a warm temperature." *Journal of Alloys and Compounds* 753 (2018): 46-53. https://doi.org/10.1016/j.jallcom.2018.04.194

[24] Azzeddine, Hiba, Djamel Bradai, Thierry Baudin, and Terence G. Langdon. "Texture evolution in high-pressure torsion processing." *Progress in Materials Science* 125 (2022): 100886. https://doi.org/10.1016/j.pmatsci.2021.100886

[25] Han, Jae-Kyung, Xiaojing Liu, Isshu Lee, Yulia O. Kuzminova, Stanislav A. Evlashin, Klaus-Dieter Liss, and Megumi Kawasaki. "Structural evolution during nanostructuring of additive manufactured 316L stainless steel by high-pressure torsion." *Materials Letters* 302 (2021): 130364. https://doi.org/10.1016/j.matlet.2021.130364

[26] Thorvaldsen, A. "The intercept method—1. Evaluation of grain shape." *Acta materialia* 45, no. 2 (1997): 587-594. https://doi.org/10.1016/S1359-6454(96)00197-8

[27] Melia, Michael A., Hai-Duy A. Nguyen, Jeffrey M. Rodelas, and Eric J. Schindelholz. "Corrosion properties of 304L stainless steel made by directed energy deposition additive manufacturing." *Corrosion Science* 152 (2019): 20-30. https://doi.org/10.1016/j.corsci.2019.02.029

[28] Qiu, Chunlei, Mohammed Al Kindi, Aiman Salim Aladawi, and Issa Al Hatmi. "A comprehensive study on microstructure and tensile behaviour of a selectively laser melted stainless steel." *Scientific reports* 8, no. 1 (2018): 7785. https://doi.org/10.1038/s41598-018-26136-7

[29] Wan, H. Y., Z. J. Zhou, C. P. Li, G. F. Chen, and G. P. Zhang. "Effect of scanning strategy on mechanical properties of selective laser melted Inconel 718." *Materials Science and Engineering: A* 753 (2019): 42-48. https://doi.org/10.1016/j.msea.2019.03.007

[30] Bertoli, Umberto Scipioni, Benjamin E. MacDonald, and Julie M. Schoenung. "Stability of cellular microstructure in laser powder bed fusion of 316L stainless steel." *Materials Science and Engineering: A* 739 (2019): 109-117. https://doi.org/10.1016/j.msea.2018.10.051

[31] Polonsky, Andrew T., McLean P. Echlin, William C. Lenthe, Ryan R. Dehoff, Michael M. Kirka, and Tresa M. Pollock. "Defects and 3D structural inhomogeneity in electron beam additively manufactured Inconel 718." *Materials Characterization* 143 (2018): 171-181. https://doi.org/10.1016/j.matchar.2018.02.020

[32] Leicht, Alexander, Uta Klement, and Eduard Hryha. "Effect of build geometry on the microstructural

development of 316L parts produced by additive manufacturing." *Materials Characterization* 143 (2018): 137-143. https://doi.org/10.1016/j.matchar.2018.04.040

[33] Wang, Jingtao, Zenji Horita, Minoru Furukawa, Minoru Nemoto, Nikolai K. Tsenev, Ruslan Z. Valiev, Yan Ma, and Terence G. Langdon. "An investigation of ductility and microstructural evolution in an Al− 3% Mg alloy with submicron grain size." *Journal of materials research* 8, no. 11 (1993): 2810-2818. https://doi.org/10.1557/JMR.1993.2810

[34] Yusuf, Shahir Mohd, Ying Chen, Shoufeng Yang, and Nong Gao. "Microstructural evolution and strengthening of selective laser melted 316L stainless steel processed by high-pressure torsion." *Materials Characterization* 159 (2020): 110012. https://doi.org/10.1016/j.matchar.2019.110012

[35] Sames, William J., F. A. List, Sreekanth Pannala, Ryan R. Dehoff, and Sudarsanam Suresh Babu. "The metallurgy and processing science of metal additive manufacturing." *International materials reviews* 61, no. 5 (2016): 315-360. https://doi.org/10.1080/09506608.2015.1116649

[36] Gu, Dong Dong, Wilhelm Meiners, Konrad Wissenbach, and Reinhart Poprawe. "Laser additive manufacturing of metallic components: materials, processes and mechanisms." *International materials reviews* 57, no. 3 (2012): 133-164. https://doi.org/10.1179/1743280411Y.0000000014

[37] Pham, M. S., B. Dovgyy, and P. A. Hooper. "Twinning induced plasticity in austenitic stainless steel 316L made by additive manufacturing." *Materials Science and Engineering: A* 704 (2017): 102-111. https://doi.org/10.1016/j.msea.2017.07.082

[38] Kawasaki, Megumi, Roberto B. Figueiredo, Yi Huang, and Terence G. Langdon. "Interpretation of hardness evolution in metals processed by high-pressure torsion." *Journal of Materials Science* 49 (2014): 6586-6596. https://doi.org/10.1007/s10853-014-8262-8

[39] Tian, Y. Z., S. D. Wu, Z. F. Zhang, R. B. Figueiredo, N. Gao, and T. G. Langdon. "Strain hardening behavior of a two-phase Cu–Ag alloy processed by high-pressure torsion." *Scripta Materialia* 65, no. 6 (2011): 477-480. https://doi.org/10.1016/j.scriptamat.2011.06.004

[40] Edalati, Kaveh, Tadayoshi Fujioka, and Zenji Horita. "Evolution of mechanical properties and microstructures with equivalent strain in pure Fe processed by high pressure torsion." *Materials transactions* 50, no. 1 (2009): 44-50. https://doi.org/10.2320/matertrans.MD200812

[41] Kang, Ji Yun, Jung Gi Kim, Hyo Wook Park, and Hyoung Seop Kim. "Multiscale architectured materials with composition and grain size gradients manufactured using high-pressure torsion." *Scientific reports* 6, no. 1 (2016): 26590. https://doi.org/10.1038/srep26590

[42] He, Qiong, Wei Wei, Ming-Sai Wang, Feng-Jiao Guo, Yu Zhai, Yan-Fei Wang, and Chong-Xiang Huang. "Gradient microstructure design in stainless steel: a strategy for uniting strength-ductility synergy and corrosion resistance." *Nanomaterials* 11, no. 9 (2021): 2356. https://doi.org/10.3390/nano11092356

[43] Mao, Qingzhong, Xiang Chen, Jiansheng Li, and Yonghao Zhao. "Nano-gradient materials prepared by rotary swaging." *Nanomaterials* 11, no. 9 (2021): 2223. https://doi.org/10.3390/nano11092223

[44] Shang, Zhongxia, Tianyi Sun, Jie Ding, Nicholas A. Richter, Nathan M. Heckman, Benjamin C. White, Brad L. Boyce, Khalid Hattar, Haiyan Wang, and Xinghang Zhang. "Gradient nanostructured steel with superior tensile plasticity." *Science Advances* 9, no. 22 (2023): eadd9780. https://doi.org/10.1126/sciadv.add9780